The IR spectrum of 12C2H2: line intensity measurements in the 1.4 μm region and update of the databases

David Jacquemart, Nelly Lacome, Jean-Yves Mandin, Victor Dana, Ha Tran, Fathou K. Gueye, Oleg M. Lyulin, Valery I. Perevalov, Laurence Régalia-Jarlot

The IR spectrum of $^{12}C_2H_2$: line intensity measurements in the 1.4 μm region and update of the databases

D. Jacquemart [a, b,*], N. Lacome [a, b], J.-Y. Mandin [c, d], V. Dana [c, d], H. Tran [c, d,1], F.K. Gueye [c, d], O.M. Lyulin [e], V.I. Perevalov [e], L. Régalia-Jarlot [f]

[a] *UPMC Univ Paris 06, UMR 7075, Laboratoire de Dynamique Interactions et Réactivité, Case courrier 49, Bât. F 74, 4, place Jussieu, 75252 Paris Cedex 05, France*

[b] *CNRS, UMR 7075, Laboratoire de Dynamique Interactions et Réactivité, Case courrier 49, Bât. F 74, 4, place Jussieu, 75252 Paris Cedex 05, France*

[c] *UPMC Univ Paris 06, UMR 7092, Laboratoire de Physique Moléculaire pour l'Atmosphère et l'Astrophysique, Case courrier 76, 4, place Jussieu, 75252 Paris Cedex 05, France*

[d] *CNRS, UMR 7092, Laboratoire de Physique Moléculaire pour l'Atmosphère et l'Astrophysique, Case courrier 76, 4, place Jussieu, 75252 Paris Cedex 05, France*

[e] *Laboratory of Theoretical Spectroscopy, Institute of Atmospheric Optics, Siberian Branch, Russian Academy of Sciences, 1, Akademicheskii av.,634055 Tomsk, Russian Federation*

[f] *Groupe de Spectrométrie Moléculaire et Atmosphérique, CNRS, UMR 6089, Université de Reims-Champagne-Ardenne, Faculté des Sciences, BP 1039, 51687 Reims Cedex 2, France*

Received 2008

[*] Corresponding author. Tel.: + 33-1-44-27-36-82; fax: + 33-1-44-27-30-21.
E-mail address: jacquemart@spmol.jussieu.fr (D. Jacquemart).
[1] Presently at Laboratoire Inter-Universitaire des Systèmes Atmosphériques, Universités Paris 12 et Paris 7, CNRS, UMR 7583, 61, avenue du Général-de-Gaulle, 94010 Créteil Cedex, France.

Abstract

Spectroscopic data are noticeably enriched in six spectral regions of the main isotopologue $^{12}C_2H_2$ of the acetylene molecule, namely, in the regions around 3, 2.2, 1.9, 1.7, 1.5, and 1.4 μm. Among these regions, only those at 3 and 1.5 μm were already presented partly in the databases. The results of line intensity measurements, performed for the first time in the 1.4 μm region, are given. Data available in the literature, or obtained in the present work, are compiled to set up line lists usable for applications in the quoted spectral regions. On the whole, 5748 new lines pertaining to 65 bands can be added to the databases.

Keywords: Acetylene; Infrared; Vibro-rotational transitions; Line parameters; Databases

1. Introduction

A review of the acetylene spectroscopic parameters in the HITRAN database was given in a paper by Jacquemart et al [1] in 2003. Last issues of databases are HITRAN 2004 [2] and GEISA 2003 [3,4]. HITRAN 2004 was enriched by the results of El Hachtouki and Vander Auwera [5] in the 1.5 µm region, which is an important spectral domain since it occurs in the emission range of telecom diode lasers. In the beginning of 2007, new line lists were added in the HITRAN database as update, in the 3.8 and 2.5 µm regions where line intensity measurements had been done [6,7]. Despite these important improvements, databases are far from to be updated. Indeed, other recent line intensity measurements have been performed but have not yet been put in the appropriate form to be included in databases. Five spectral regions of acetylene are thus concerned, the regions at 3 µm [1,8,9], 2.2 [10], 1.9 [11], 1.7 [11], and 1.5 µm [12,13]. The goal of this work is to set up line lists in these five regions, usable for atmospheric or astrophysical applications. Data existing in databases have been completed, using band-by-band effective models based on polynomial adjustments of line positions and intensities. The aim of such lists is to help for current applications, not to propose a complete synthetic spectrum that more powerful models will be able to produce in some years. A sixth spectral region, at 1.4 µm, has been also investigated in the present work. More than 230 line intensities have been measured in this region, and a line list has also been produced to be put in databases. Section 2 of the paper reports results obtained around 1.4 µm from Fourier transform spectra recorded both at GSMA (Reims) and at LADIR (Paris). Section 3 presents in details the content of the line lists and how they have been set up in each spectral region. In the Conclusion we list the data of atmospheric and astrophysical interest which still have to be added to databases. In the remaining of the paper, databases refer specifically to the HITRAN and GEISA databases.

2. $^{12}C_2H_2$ line intensity measurements in the 1.4 µm spectral region

2.1. Introduction

The 1.4 µm spectral region of $^{12}C_2H_2$ concerns the $\Delta P = 11$ sequence of vibrational transitions. According to [14] and [15], we have noted P the pseudo-quantum number equals to $5v_1 + 3v_2 + 5v_3 + v_4 + v_5$, where v_1, v_2, v_3, v_4, and v_5 are the quantum numbers associated with the normal modes of vibration of the molecule. A given value of P is assigned to a given set of interacting vibrational states, named polyad or cluster. Polyads are also noted $\{Pv_5\}$. In this frame, global vibration and vibration-rotation analysis were performed [16-19]. Throughout this paper, we will use the vibrational notations of Plíva [20,21] adopted in the HITRAN database [2,22]. Thus, vibrational levels are noted $v_1\ v_2\ v_3\ (v_4\ v_5)^{\ell}_{\pm}\ r$, with $\ell = |\ell_4 + \ell_5|$, ℓ_t being the vibrational angular momentum quantum number associated with the degenerated bending mode t, $\pm$ being the symmetry type for Σ vibrational states ($\ell = 0$), and r a roman numeral indicating the rank of the level, by decreasing energy value (r = I for the highest energy level), inside the set of states having the same vibrational symmetry, and coupled by ℓ-type resonances. The last work performed on the 1.4 µm spectral region is that of Vander Auwera et al [23], who measured absolute line wavenumbers in four cold bands and deduced spectroscopic parameters for the involved vibrational levels. Their work was undertaken mainly to help metrological applications in the field of optical fiber communication systems. The accuracy of the measured wavenumbers is between 0.0003 and 0.006 cm^{-1} depending on the line. As far as line intensities are concerned, no data have been published to our knowledge, except for a prediction of band intensities for two bands around 7200 cm^{-1}, by Abbouti Temsamani et al [24]. Note that databases do not contain any data for $^{12}C_2H_2$ around 1.4 µm.

The four cold bands observed by Vander Auwera et al [23], and that we also observed in our spectra, are listed in Table 1. Since these perpendicular bands are all of $\Pi_u \leftarrow \Sigma^+_g$ type, they

exhibit the same structure with a strong *Q*-branch and a 3:1 intensity alternation ratio, according to odd:even *J*, *J* being the rotational quantum number of the lower level.

2.2. Experimental details

To study the C_2H_2 1.4 μm spectral region, 15 spectra were obtained with the GSMA (Reims) step-by-step interferometer [25,26]. Experimental conditions are gathered in Table 2. The apparatus was used with a tungsten radiation source, SiO_2 splitting and mixing plates, InSb detectors, and CaF_2 cell windows. Pressures were measured using two full scale ranges MKS Baratrons (10- and 100-Torr manometers) with an accuracy of 0.5%. Spectra number 1-10 of Table 2 had already been used to study the 1.5 μm region [12,13], whereas spectra number 11-15 are new spectra recorded with a shorter length cell, in order to better observe strong lines around 7200 cm^{-1}.

Nine additional spectra were obtained with the rapid scan Bruker IFS 120 HR interferometer of the LADIR (Paris). Experimental conditions are gathered in Table 3. This interferometer was equipped with a Globar source, CaF_2 beam splitter, an InSb detector, and an optical filter covering the 500-12500 cm^{-1} spectral region. The whole optical path was under vacuum and a multipass cell of 1-m base length was used. The cell was equipped with KCl windows. The temperature of the gas in the cell was recorded via four platinum probes at different places inside the cell. The uncertainty on the temperature measurements has been estimated to be ±0.5 K. Pressures were measured using two full scale ranges MKS Baratrons (10- and 100-Torr manometers) with an accuracy of 0.5%. Each scan among at least 390 recorded for every spectrum has then been individually transformed to a spectrum using the Fourier transform procedure included in the Bruker software OPUS package [27], selecting a Mertz phase error correction [28,29].

Note that the acetylene samples used in Reims and Paris were obtained from the same company, but became from different cylinders.

2.3. Method of measurement

To obtain the $^{12}C_2H_2$ line intensities in the 7200 cm^{-1} spectral region, we had at our disposal two sets of spectra recorded using two different spectrometers. Since these two sets of spectra are recorded at similar experimental conditions, the multispectrum procedure [30] used to derive line intensities can be performed by merging these sets. However, before running the procedure, we had to check that such a way to proceed is correct and does not induce systematic errors [31]. A sample of 50 lines has been chosen between 6600 and 7500 cm^{-1}, and their intensities have been obtained using GSMA and LADIR spectra separately. The average difference between the GSMA and LADIR results is (0.74 ± 1.30)%, with 1 SD after the $\pm$ sign. This very good agreement entitles us to use the multispectrum procedure with the whole set of spectra. Let us recall that line intensities measured in the 6600 cm^{-1} spectral region from the GSMA spectra [12] were also found in very good agreement with those of El Hachtouki and Vander Auwera [5], i.e., (0.20 ± 0.64)%. The mean accuracy of absolute line intensities reported in this paper is estimated to be between 3 and 5% for most of the lines, but it can be worse than 10% for some very weak lines, or in the case of strong overlappings, especially in *Q*-branches.

Practically, the multispectrum procedure was used exactly in the same way as in [12], so that we will recall here only what is important. First, spectra were prepared as in [12]: adjustment of an effective value of the iris radius for each spectrum, determination of the phase error for the GSMA spectra, and calibration of the absolute wavenumber scale of each spectrum. Then, the multispectrum procedure was run in the following conditions. A Voigt profile was used to calculate the absorption coefficient of the lines, and the self-broadening coefficients were

fixed at the values calculated according to [32]. The self-shifting coefficients were fixed at zero. On the whole, 233 line intensities have been measured in 4 bands. These results are listed in Table 4.

As far as line positions are concerned, let us recall that the wavenumber scale of the GSMA spectra had been calibrated as explained in [12]. For the LADIR spectra, the accurate absolute positions of 22 well isolated lines measured by Vander Auwera et al [23] have been used, the standard deviation of the fit being smaller than 0.0001 cm^{-1}.

2.4. Results and data reduction

For each line intensity $S(T_0)$ obtained from the multispectrum fitting procedure, in $cm \cdot molecule^{-1}$ at the standard temperature T_0 = 296 K, we used the following formula to deduce the transition dipole moment squared $|R|^2$, in D^2 (1 debye = 3.33546×10^{-30} C·m)

$$S(T_0) = (1/4\pi\varepsilon_0)\,(8\pi^3/3hc)\,[g''\nu_0/Q(T_0)]\,|R|^2\,L(J,\ell)\,\exp(-hcE''/kT_0)\,[1-\exp(-hc\,\nu_0/kT_0)], \qquad (1)$$

where $1/4\pi\varepsilon_0 = 10^{-36}$ erg·cm^3·D^{-2}; h is Planck's constant equal to $6.6260755 \times 10^{-27}$ erg·s (1 erg = 10^{-7} J); c is the speed of light in vacuum equal to $2.99792458 \times 10^{10}$ cm·s^{-1}; g'' is the statistical weight due to nuclear spin of the lower level (1 for *s*-type levels and 3 for *a*-type levels); ν_0 is the transition wavenumber in cm^{-1}; $Q(T_0)$ is the total partition function at temperature T_0; $L(J,\ell)$ is the Hönl-London factor; E'', in cm^{-1}, is the energy of the lower level; k is Boltzmann's constant equal to 1.380658×10^{-16} erg·K^{-1}. For perpendicular bands ($\Delta\ell = \pm 1$), the Hönl-London factors are given by

$$L(J,\ell) = (J+2+\ell\Delta\ell)\,(J+1+\ell\Delta\ell)\,/\,[2(J+1)] \quad (R\text{-branch}), \qquad (2)$$

$$L(J,\ell) = (J+1+\ell\Delta\ell)\,(J-\ell\Delta\ell)\,(2J+1) / [2J(J+1)] \quad (Q\text{-branch}), \tag{3}$$

$$L(J,\ell) = (J-1-\ell\Delta\ell)\,(J-\ell\Delta\ell) / (2J) \quad (P\text{-branch}). \tag{4}$$

In Eq. (1), the E'' energy values of the ground state have been taken from HITRAN [2]. We used the partition function of Fischer et al [33].

To reduce the data, effective parameters can be deduced expanding $|R|^2$ empirically to take into account the rotational dependence

$$|R|^2 = |R_0|^2\,(1 + A_1^{\,RP}\, m + A_2^{\,RP}\, m^2)^2 \quad (P\text{- and } R\text{-branches}), \tag{5}$$

$$|R|^2 = |R_0|^2\,(1 + A_2^{\,Q}\, m^2)^2 \quad (Q\text{-branch}), \tag{6}$$

m being equal to $-J$ in the P-branch, J+1 in the R-branch, and J in the Q-branch. $|R_0|^2$ is the vibrational transition dipole moment squared, and $A_1^{\,RP}$, $A_2^{\,RP}$, and $A_2^{\,Q}$, Herman-Wallis coefficients. Note that the terms between parentheses in Eqs. (5,6) are squared in the present work.

Vibrational transition dipole moment squared values and Herman-Wallis coefficients deduced from an unweighted fit of the experimental $|R|^2$ values are reported in Table 5. An example is plotted in Fig. 1 for the $2\nu_1 + \nu_5^{\,1}$ band. The large relative differences between measured and calculated $|R|^2$ values, observed at the end of the P- and R-branches of the ν_1 +

$\nu_2 + (2\nu_4 + \nu_5)^1$ band (see Table 4), are the consequence of measurements carried out for weak to very weak lines, therefore characterized by a lower precision.

A synthetic spectrum can now be calculated using the constants of Table 5. For the sake of coherence, the set up of the line list in the 1.4 μm region will be described in the next Section.

3. Calculation of the line lists for the databases

3.1. General considerations

Our aim was to set up the line lists useful for the practical applications. For these purposes we did our best to take into account a maximum of published data. When accurate absolute line positions or line intensities were already published, we have picked up these values as they were published. The accuracy of these line positions is usually between 0.0003 and 0.006 cm^{-1} (see, e.g., [23]), and that of line intensities is better than 2% (see, e.g., [5,34]). In some cases, effective polynomial expansions of line positions have been performed to interpolate or slightly extrapolate the experimental sample of values, in order to obtain complete usable line lists. Uncertainty codes for extrapolated data have then been degraded. When an extrapolation has been performed, we have limited it to the maximum measured *J* value, often increased by about 5. For extrapolated lines, the uncertainty codes have been degraded (for example 10% instead of 5% for line intensities). As for a band, most of the transitions have a similar code (e.g., 5%), extrapolated ones (having, e.g., 10%) are easily recognizable. When no absolute values were measured, calculated line positions have been generated through effective polynomial expansions of available measured positions. Except for very few cases, which will be quoted in the next sub-sections, this method is precise enough for our purpose: residuals are at most a few 10^{-3} cm^{-1}.

Empirical Herman-Wallis factors have been used to calculate the line intensities. Except for a few cases, concerning mainly weak bands, this model is precise enough to well reproduce experimental intensities in a view to atmospheric or astrophysical applications. Practically, the transition moments squared $|R|^2$ have been calculated using the vibrational transition moments squared $|R_0|^2$ and the Herman-Wallis coefficients reported in the original papers, the Herman-Wallis factor being expanded as in the quoted works. Details on these calculations can be found in the original papers. Since the total partition function calculated by Gamache et al [35] had been used in some of these works, we used it again to retrieve the concerned line intensities from the $|R|^2$ values using Eq. (1). Note that, for all $^{12}C_2H_2$ data presented in the databases the Einstein *A*-coefficients mentioned in the line lists are those obtained with the updated partition function given by Fischer et al [33], though the difference between the two values is very weak (smaller than 0.37% at 296 K). When it seemed to us possible to extrapolate slightly the line intensity calculation with respect to the set of experimental values, the rotational dependence of the transition moment squared $|R|^2$ has been neglected for the extrapolated intensities, thus the calculation has been performed fixing $|R|^2$ to the $|R|^2$ value calculated for the last measured line. Note that the concerned lines are often very weak, and that the uncertainty codes of their positions and intensities have been consequently degraded.

For the sake of simplicity, line intensities and $|R|^2$ values have been listed respecting the HITRAN format, i.e., with 4 digits, $|R|^2$ values being put instead of Einstein-*A* coefficients. Of course, these digits are not always significant since the mean accuracy is around 5%, and can be degraded up to more than 10% for very weak lines, for extrapolated intensity values, or for a few bands for which the empirical Herman-Wallis model appears not well adapted. Consequently, listed values, when calculated, could differ by a few thousandth from those that were published with 3 significant digits, because of truncations or roundings. Therefore, the readers who whish to know the exact values of the measured intensities are referred to the quoted papers. Energy

values of the lower vibro-rotational levels of the transitions have been taken from the HITRAN 2004 file, in the 13.6 µm spectral region. If not available in this file, they have been deduced from the results of Kabbadj et al [36]. Note that the differences between E" values obtained from various sources are totally negligible for intensity calculations at temperatures other than 296K. The other spectroscopic data are the same as those already put in the last updates of the databases: air- and self-broadening coefficients, default value for the temperature exponent of air-broadening coefficients, constant value for the air-pressure shifting coefficient, and their accuracies [2,6,22].

The present work only concerns the main isotopologue $^{12}C_2H_2$. The upper plot of Fig. 2 shows the acetylene transitions present in the current version of HITRAN, with its last updates, their intensities being displayed vs. wavenumber. This figure shows that there is a lack of data in numerous spectral domains. Table 6 gathers the information of Fig. 2 together with the new data introduced by the present work. The first part of this table synthetises the whole data now available for C_2H_2, and the second part summarises details concerning the spectral regions and bands newly studied or updated in the present work. What we have done to set up a line list in each spectral region is detailed in the following sub-sections.

As far as the previous updates of 2007 (the 2.5 and 3.8 µm regions) are concerned, an exhaustive explanation has been given in the Appendix of [6] for the 3.8 µm region, but nothing has been published for the 2.5 µm region [7]. As the 2.5 µm line list has been set up exactly in the same way as for the 3.8 µm region, we will refer the reader to [6], and we will only recall that vibrational transition dipole moments squared and Herman-Wallis coefficients were taken from Table 12 of [7], and were used according to Eqs. (1-6) of [7]. The *Q*-branch of the $\nu_3 + \nu_4^1$ band received a special treatment, see Eq. (7) of [7], and as it was erroneous both for positions and intensities in the update of 2007, it has been recalculated and corrected in the new version. Furthermore, an error is present in Table 4 of [7] for $|R|^2$ values of these *Q* lines, so that the plot

of *Q* lines in Fig. 2 of [7] is wrong. Table 7 gives corrected values to put in place of those of the corresponding lines in [7]. For this *Q* branch, the $A_1{}^Q$ value given in Table 12 of [7] is erroneous too: the true value to take into account is $A_1{}^Q = -4.78(20) \times 10^{-3}$. Let us recall that the *Q*-branch of the $\nu_2 + (2\nu_4 + \nu_5)^1$ II band could not be calculated because it is too confined to allow line position and line intensity measurements, but its integrated absorption coefficient could be measured: 0.749 ± 0.040 cm^{-2}·atm^{-1} at 296 K. Furthermore, a few errors in vibrational and rotational assignments, without consequences for applications, have been corrected.

3.2. The 3 µm spectral region

In this spectral region, the databases already contained line positions and intensities from Vander Auwera et al [37] for the two strong bands ν_3 and $\nu_2 + (\nu_4 + \nu_5)^0{}_+$. Let us recall that line intensities of [37] and those obtained in [1] were found in very good agreement, namely (0.5 ± 1.5)% and (0.6 ± 1.7)% respectively for ν_3 and $\nu_2 + (\nu_4 + \nu_5)^0{}_+$. For these two bands, data present in the databases were not changed. For the other bands, line positions retained for the line list are those that Rinsland et al [38] calculated from their measured values, by using effective polynomial expansions. A systematic discrepancy of 0.0012 cm^{-1} between line positions of [37] and [38] has been observed. Consequently, line positions calculated from [38] have been decreased by 0.0012 cm^{-1}. We have limited each branch to the maximum *J* value observed by Rinsland et al, namely J_{obs}, so that, as in [38], we have not performed extrapolation for line positions. However, as more lines were observed in [38] than in [37], the two bands present in the databases have been extrapolated from $J = 40$ up to $J = 50$, line positions being calculated as said above, and line intensities calculated using the vibrational transition moments squared $|R_0|^2$ and Herman-Wallis coefficients obtained in [8], that we had found very close to those of [37] and [38]. Note that for these two particularly important bands, the intensity

extrapolation has been attempted up to 10 supplementary J values, instead of about 5 for the other bands.

As far as line intensities of other bands are concerned, they have been calculated using $|R_0|^2$ and Herman-Wallis coefficients obtained in [8,9], the Herman-Wallis factor being expanded according to Eq. (4) of [8]. To calculate line intensities, the total partition function of Gamache et al [35] has been used as in [8,9]. Taking into account the sample of line intensities measured in each band, this calculation has been extrapolated only up to a J_{max} value (between about 15 and 40) depending on the band (J_{max} being smaller than J_{obs}). Beyond J_{max} and up to J_{obs}, the calculation has been performed fixing $|R|^2$ to the constant value $|R|^2(J_{max})$. Note that for several bands of the 3 µm spectral region, the extrapolation has to be performed over almost 20 values of J, particularly for the two strong bands ν_3 and $\nu_2 + (\nu_4 + \nu_5)^0_+$.

Our line list now contains 2000 additional lines around 3 µm. Thus updated, the databases should allow a noticeable improvement in the analysis of cool carbon star spectra [38].

3.3. The 2.2 µm spectral region

Data concerning this spectral region do not exist in databases. Main references about the 2.2 µm spectral region can be found in a recent work [10] in which line positions and intensities were measured for 444 lines of 8 bands. In [10], vibrational transition dipole moments squared and Herman-Wallis coefficients were determined only for 2 bands. Indeed, because of strong interactions that lead to unusual rotational dependences of the transition dipole moments squared, the Herman-Wallis factor model is not always well adapted. However, for the purpose of the present work, this model has been used for the 6 remaining bands, to reduce line intensity data with enough precision. Effective vibrational transition dipole moments squared and Herman-Wallis coefficients have been obtained through Eq. (4) of [10]. They are given in Table 8. Note

that for $\Pi \leftarrow \Pi$ bands, experimental data of *ee* and *ff* sub-bands have been adjusted simultaneously.

To build the line list, line positions have been calculated from empirical polynomial fits of the measured line positions of [10], issued from a multispectrum adjustment procedure. A few missing lines were then interpolated, and an extrapolation has been performed, adding about 5 lines to the last measured one (namely J_{obs}), so that J_{max} is equal to 25, 30, or 35, depending on the band. For high J values, and for a few interpolated lines of the $\nu_3+3\nu_4^1 - \nu_4^1$ band, the uncertainty code has been degraded. Up to J_{obs}, line intensites have been calculated using $|R_0|^2$ and Herman-Wallis coefficients of Table 11 of [10] and Table 8 of this paper, the Herman-Wallis factor being expanded according to Eq. (4) of [10]. To calculate line intensities, the total partition function of Gamache et al [35] has been used as in [10]. The calculation has been extrapolated up to J_{max}, but beyond J_{obs}, $|R|^2$ has been fixed to the constant value $|R|^2(J_{obs})$. The uncertainty code of the intensity of high J lines has been degraded.

3.4. The 1.9 and 1.7 µm spectral regions

Databases do not contain information in the 1.9 and 1.7 µm spectral regions of C_2H_2. Recently, these two regions were studied from a single campaign of measurements [11]. Line intensities were derived for 13 bands for which vibrational transition dipole moments squared and Herman-Wallis coefficients could be obtained, see Table 9 of [11]. Around 5900 cm^{-1}, line positions measured in [11] were found in very good agreement with those obtained by Keppler et al [39]. Consequently, line positions of [11] have been used to generate a line list through empirical polynomial adjustments. However, for bands for which more lines were observed in [39] than in [11], line positions of [39] have been preferred for these adjustments. Line intensities have been calculated using the constants of Table 9 of [11] and Eqs. (20,21) of [11],

with the total partition function of Gamache et al [35] to be consistent with [11]. Note that intensities published in [11] are those resulting directly from the fit of $|R|^2$, whereas those given in the line list have been calculated using constants (see Table 9 of Ref. [11]) truncated to take into account the actual accuracy. Though the differences between these two sets of values are small (inside the announced precision), values calculated for the line list should be preferred. As for the previous spectral regions, the calculation has been performed up to a J_{max} value depending on the band (typically 20, 25, 30, or 35, according to the lines observed in [39]), but beyond the value of the last measured intensity, namely J_{obs}, $|R|^2$ has been fixed to the constant value $|R|^2(J_{obs})$. Uncertainty codes of positions and intensities of extrapolated lines have been degraded consequently.

3.5. The 1.5 µm spectral region

The 1.5 µm spectral region is an atmospheric window where acetylene is able to be observed, particularly as a pollutant in the troposphere. Then, it is useful to have a maximum of information about C_2H_2 line intensities in this region. Line positions and intensities of the 4 strongest bands, issued from accurate absolute measurements, have already been included in databases by El Hachtouki and Vander Auwera [5]. Consequently, data concerning these 4 bands have not been changed, except for the default value of the temperature exponent (0.75) that we have added. For 20 additional bands, experimental line positions obtained by Keppler et al [39] have been chosen for the databases, since their precision is better than this of current calculations, especially in case of interacting bands. However, positions of a few unobserved lines have been interpolated and reported with a degraded uncertainty code. Line intensities have been calculated according to the same principles than for the previous spectral regions. Vibrational transition dipole moments squared and Herman-Wallis coefficients of Table 4 of [12]

and of Table 3 of [13] have been used, according to Eq. (5) of [12], and with the total partition function of Fischer et al [33]. Intensities have been extrapolated up to the last line observed in [39], or to a *J* value slightly larger. Note that the uncertainty code is rather poor for a few weak hot bands whose intensities could be measured with a mean accuracy only between 10 and 20% [13]. Our line list now contains information about 24 bands around 1.5 µm.

3.6. The 1.4 µm spectral region

Line intensities obtained in this work for 4 bands (see Section 2) have been merged with the absolute line positions published by Vander Auwera et al [23] in order to get a consistent set of data. For the databases, the absolute experimental positions given in [23] have been kept with an uncertainty code 4 (accuracy between 10^{-4} and 10^{-3} cm^{-1}), except for a few lines quoted by an asterisk in [23] that have received a code 3 (accuracy between 10^{-3} and 10^{-2} cm^{-1}). For the lines not given in [23] but that could be treated in the present work, the experimental positions resulting from the multispectrum procedure have been added with a code 4. The agreement between our line positions (the spectra being calibrated) and those of Vander Auwera et al [23] is very good, the mean difference being negligible for well isolated lines (less than 10^{-6} cm^{-1}). This agreement is excellent: into a 0.0001 cm^{-1} error bar (1SD). Finally, the positions of a few lines have also been interpolated or extrapolated by usual effective polynomial fits (uncertainty code 3). Line intensites have been calculated as for the previous spectral regions, using the constants of Table 5 according to Eqs. (5,6), and with the partition function of Fischer et al [33].

4. Conclusion

Acetylene data contained in spectroscopic databases can be noticeably improved. Among the 10571 transitions of $^{12}C_2H_2$ now available for this molecule, 5748 come from the present update. They concern 63 new bands. The line list concerning the 8 spectral regions modified, extended, or added can be obtained as supplementary material attached to this paper. The lower plot of Fig. 2 shows the improvement after the present work. Despite these improvements, additional efforts have to be done to acquire more data in the remaining infrared spectral regions of $^{12}C_2H_2$, namely, in the three domains around 1.3, 1.2, and 1 μm, that are still absent in the databases. Line intensity measurements are planed for the strongest bands observed in these domains [23]. In the same way, in the 7.7 μm region, the databases contain data concerning the strong $(\nu_4 + \nu_5)^0_+$ cold band, from the work of Vander Auwera [34], but numerous other bands observed in this region by Kabbadj et al [36] would deserve to be studied and included in the databases, since the 7.7 μm region is of astrophysical interest. The case of the $\Delta P = 1$ sequence of transitions, around 13.6 μm, is also interesting since the strong ν_5^1 band, accompanied by many hot bands between 600 and 870 cm^{-1}, is often observed in atmospheric and planet spectra. Kabbadj et al [36] observed and assigned other bands of the same sequence between 440 and 570 cm^{-1}, and it would be important to take them into account in the databases.

Acknowledgements

The authors acknowledge X. Thomas, P. Von der Heyden, and D. Décatoire from Groupe de Spectrométrie Moléculaire et Atmosphérique (Reims, France) for their contribution in some parts of this work.

References

[1] Jacquemart D, Mandin JY, Dana V, Claveau C, Vander Auwera J, Herman M, Rothman LS, Régalia-Jarlot L, Barbe V. The IR acetylene spectrum in HITRAN: update and new results. JQSRT 2003;82:363-82.

[2] Rothman LS, Jacquemart D, Barbe A, Benner DC, et al. The Hitran 2004 Molecular Spectroscopic Database. JQSRT 2005;96:139-204.

[3] Jacquinet-Husson N, Scott NA, Chédin A, Garceran K, et al. The 2003 edition of GEISA / IASI spectroscopic database. JQSRT 2005;95:429-67.

[4] Jacquinet-Husson N, Scott NA, Chédin A, Crépeau L, et al. The GEISA spectroscopic database : current and future archive for Earth's planetary atmosphere studies. JQSRT 2008;109:1043-59.

[5] El Hachtouki R, Vander Auwera J. Absolute line intensities in acetylene: the 1.5 µm region. J Mol Spectrosc 2002;216:355-62.

[6] Jacquemart D, Lacome N, Mandin JY, Dana V, Lyulin OM, Perevalov VI. Multispectrum fitting procedure for $^{12}C_2H_2$ in the 3.8-µm spectral region. JQSRT 2007;103:478-95.

[7] Lyulin OM, Perevalov VI, Mandin JY, Dana V, Gueye F, Thomas X, Von der Heyden P, Décatoire D, Régalia-Jarlot L, Jacquemart D, Lacome N. Line intensities of acetylene:

measurements in the 2.5-μm spectral region and global modeling in the $\Delta P = 4$ and 6 series. JQSRT 2007;103:496-523.

[8] Mandin JY, Jacquemart D, Dana V, Régalia-Jarlot L, Barbe A. Line intensities of acetylene at 3 μm. JQSRT 2005;92:239-60.

[9] Lyulin OM, Perevalov VI, Mandin JY, Dana V, Jacquemart D, Regalia-Jarlot L, Barbe A. Line intensities of acetylene in the 3-μm region: New measurements of weak hot bands and global fitting. JQSRT 2006;97:81-98.

[10] Lyulin OM, Perevalov VI, Gueye F, Mandin JY, Dana V, Thomas X, Von der Heyden P, Régalia-Jarlot L, Barbe A. Line positions and intensities of acetylene in the 2.2-μm region. JQSRT 2007;104:133-54.

[11] Lyulin OM, Jacquemart D, Lacome N, Perevalov VI, Mandin JY. Line parameters of acetylene in the 1.9 and 1.7-μm spectral regions. JQSRT 2008;109:1856-74.

[12] Tran H, Mandin JY, Dana V, Régalia-Jarlot L, Thomas X, Von der Heyden P. Line intensities in the 1.5-μm spectral region of acetylene. JQSRT 2007;108:342-62.

[13] Lyulin OM, Perevalov VI, Tran H, Mandin JY, Dana V, Régalia-Jarlot L, Thomas X, Décatoire D. Line intensities of acetylene: New measurements in the 1.5-μm spectral region and global approach in the $\Delta P = 10$ series. JQSRT submitted for publication.

[14] Kelman ME, Gengxin C. Approximate constants of motion and energy transfer pathways in highly excited acetylene. J Chem Phys 1991;95:8671-2.

[15] Perevalov VI, Lobodenko EI, Teffo JL. Reduced effective Hamiltonian for global fitting of C_2H_2 rovibrational lines. In: Proceedings of the XIIth Symposium and school on high-resolution molecular spectroscopy. St. Petersburg, Russian Federation. SPIE 1997;3090:143-9.

[16] Herman M, Liévin J, Vander Auwera J, Campargue C. Global and accurate vibration Hamiltonians from high-resolution molecular spectroscopy. Adv Chem Phys 1999;108:1-431. Wiley, New York.

[17] Lyulin OM, Perevalov VI, Teffo JL. Global fitting of vibration-rotation line positions of acetylene molecule in the far and middle infrared regions. In: Proceedings of the 14th Symposium on High-Resolution Molecular Spectroscopy. Krasnoyarsk, Russian Federation. SPIE 2004;5311:134-43.

[18] Herman M, Campargue C, El Idrissi MI, Vander Auwera J. Vibrational spectroscopic database on acetylene, $X\,^1\Sigma^+_g$ ($^{12}C_2H_2$, $^{12}C_2D_2$, and $^{13}C_2H_2$). J Phys Chem Ref Data 2003;32:921-1361.

[19] Robert S, Amyay B, Herman M, Fayt A. Global vibration-rotation analysis in acetylene $^{12}C_2H_2$ and astrophysical applications. In: Abstracts of the 20th colloquium on High-Resolution Molecular Spectroscopy. Dijon, France 2007: p.140.

[20] Plíva J. Spectrum of acetylene in the 5-micron region. J Mol Spectrosc 1972;44:145-64.

[21] Plíva J. Molecular constants for the bending modes of acetylene $^{12}C_2H_2$. J Mol Spectrosc 1972;44:165-82.

[22] Šimečková M, Jacquemart D, Rothman LS, Gamache RR, Goldman A. Einstein *A*-coefficients and statistical weights for molecular absorption transitions in the HITRAN database. JQSRT 2006;98:130-55.

[23] Vander Auwera J, El Hachtouki R, Brown LR. Absolute line wavenumbers in the near infrared: $^{12}C_2H_2$ and $^{12}C^{16}O_2$. Mol Phys 2002;100:3563-76.

[24] Abbouti Temsamani M, Champion JM, Oss S. Infrared transition intensities in acetylene: an algebraic approach. J Chem Phys 1999 ;110 :2893-902.

[25] Plateaux JJ, Barbe A, Delahaigue A. Reims high resolution Fourier transform spectrometer. Data reduction for ozone. Spectrochim Acta 1995;51A:1153-69.

[26] Régalia L. Mesures à l'aide d'un spectromètre par transformation de Fourier, des intensités et coefficients d'élargissement de molécules d'intérêt atmosphérique. Étude des précisions: application à N_2O, H_2O, O_3. Thèse, Université de Reims-Champagne-Ardenne, Reims, France, 1996.

[27] Wartewig S. IR and Raman Spectroscopy: Fundamental Processing. Weinheim: Wiley-VCH; 2003.

[28] Mertz L. Transformations in Optics. New York: Wiley; 1965.

[29] Griffiths PR, deHaseth JA. Fourier Transform Infrared Spectrometry. New York: Wiley; 1986.

[30] Jacquemart D, Mandin JY, Dana V, Picqué N, Guelachvili G. A multispectrum fitting procedure to deduce molecular line parameters. Application to the 3–0 band of $^{12}C^{16}O$. Eur Phys J D 2001;14:55-69.

[31] Mandin JY, Dana V, Jacquemart D, Lacome N, Régalia-Jarlot L, Barbe A, Thomas X, Von der Heyden P. Some difficulties of a multilaboratory multispectrum fitting procedure. Proceedings of the VIIth Atmospheric Spectroscopy Applications Colloquium, Reims, 6-8 september 2005, Groupe de Spectrométrie Moléculaire et Atmosphérique, Ed., Université de Reims-Champagne-Ardenne, pages 43-6.

[32] Jacquemart D, Mandin JY, Dana V, Régalia-Jarlot L, Plateaux JJ, Décatoire D, Rothman LS. The spectrum of acetylene in the 5-µm region from new line-parameter measurements. JQSRT 2003;76:237-67.

[33] Fischer J, Gamache RR, Goldman A, Rothman LS, Perrin A. Total internal partition sums for molecular species in the 2000 edition of the HITRAN database. JQSRT 2003;82:401-12.

[34] Vander Auwera J. Absolute intensities measurements in the ($\nu_4 + \nu_5$) band of $^{12}C_2H_2$: analysis of Herman-Wallis effects and forbidden transitions. J Mol Spectrosc 2000;201:143-50.

[35] Gamache RR, Kennedy S, Hawkins RL, Rothman LS. Total internal partition sums for molecules in the terrestrial atmosphere. J Mol Struct 2000;517-8:407-25.

[36] Kabbadj Y, Herman M, Di Lonardo G, Fusina L, Johns JWC. The bending energy levels of C_2H_2. J Mol Spectrosc 1991;150:535-65.

[37] Vander Auwera J, Hurtmans D, Carleer M, Herman M. The ν_3 fundamental in C_2H_2. J Mol Spectrosc 1993;157:337-57.

[38] Rinsland CP, Baldacci A, Rao KN. Acetylene bands observed in carbon stars: a laboratory study and an illustrative example of its application to IRC+10216. Astrophys J Suppl Ser 1982;49:487-513.

[39] Keppler KA, Mellau GCh, Klee S, Winnewisser BP, Winnevisser M, Plíva J, Rao KN. Precision measurements of acetylene spectra at 1.4-1.7 μm recorded with 352.5-m pathlength. J Mol Spectrosc 1996;175:411-20.

Captions of tables

Table 1
List of the bands observed in the $\Delta P = 11$ series of transitions of $^{12}C_2H_2$ around 1.4 μm

Table 2
Experimental conditions and characteristics of the spectra recorded in the 1.4-μm region using the stepping-mode interferometer in Reims (GSMA)

Table 3
Experimental conditions and characteristics of the spectra recorded in the 1.4-μm region using the rapid-scan interferometer in Paris (LADIR)

Table 4
Line positions and intensities for bands of the $^{12}C_2H_2$ molecule in the 1.4 μm region

Table 5
Summary of $^{12}C_2H_2$ experimental vibrational transition dipole moments squared $|R_0|^2$ in D^2 ($1\ D = 3.33546 \times 10^{-30}$ C·m), and Herman-Wallis coefficients, see Eqs. (5,6), for 4 bands in the 1.4 μm spectral region

Table 6
Summary of bands and transitions now available for the $^{12}C_2H_2$ molecule

Table 7
Corrected line intensities and $|R|^2$ values for some Q lines of the $\nu_3+\nu_4{}^1$ band of $^{12}C_2H_2$ in the 2.5-μm region

Table 8
Additional $^{12}C_2H_2$ experimental vibrational transition dipole moments squared $|R_0|^2$ in D^2 ($1\ D = 3.33546 \times 10^{-30}$ C·m), and Herman-Wallis coefficients, see Eq. (4) of [10], for 6 bands in the 2.2 μm spectral region

Captions of figures

Fig. 1. Variation of the transition dipole moment squared $|R|^2$, in D^2 ($1\ D = 3.33546 \times 10^{-30}$ C·m), vs. m, for the $2\nu_1 + \nu_5{}^1$ band (solid triangles are for P- and R-branches, and open triangles for the Q-branch). The solid lines have been calculated using the constants found in this work (see Table 5).

Fig. 2. Line intensity ranges in each spectral domain of $^{12}C_2H_2$ (marked by their ΔP value). Upper plot: data present in the HITRAN 2004 issue, with the updates of 2007. Lower plot: data now available for databases after the present work.

Table 1
List of the bands observed in the $\Delta P = 11$ series of transitions of $^{12}C_2H_2$ around 1.4 μm

Band	Center [a]	Upper level	Polyad [b]	Symmetry	Nb lines [c]
$2\nu_1 + \nu_5{}^1$	7417.57	$200(01)^1$	$\{11\nu_5\}$	$\Pi_u \leftarrow \Sigma^+_g$	74
$\nu_1 + \nu_2 + (2\nu_4 + \nu_5)^1$	7229.45	$110(21)^1$	$\{11\nu_5\}$	$\Pi_u \leftarrow \Sigma^+_g$	41
$2\nu_3 + \nu_5{}^1$	7219.37	$002(01)^1$	$\{11\nu_5\}$	$\Pi_u \leftarrow \Sigma^+_g$	64
$\nu_1 + \nu_3 + \nu_4{}^1$	7142.67	$101(10)^1$	$\{11\nu_5\}$	$\Pi_u \leftarrow \Sigma^+_g$	54

[a] Rough values of band centers, in cm^{-1}, compiled from [23].
[b] Polyad to which the upper vibrational level belongs.
[c] Number of line intensities measured in the present work.

Table 2
Experimental conditions and characteristics of the spectra recorded in the 1.4-μm region using the stepping-mode interferometer in Reims (GSMA)

Commercial sample (Air Liquide Alphagaz)	
Natural C_2H_2	97.760% of $^{12}C_2H_2$
Stated purity	99.55%
Maximum path difference	52 cm (spectrum 1)
	75 cm (spectra 2 to 5)
	82 cm (spectra 6 to 15)
Unapodized FWHM resolution	$\approx 9.6 \times 10^{-3}$ cm^{-1} (spectrum 1)
	$\approx 6.6 \times 10^{-3}$ cm^{-1} (spectra 2 to 5)
	$\approx 6.1 \times 10^{-3}$ cm^{-1} (spectra 6 to 15)
Spectral step after post-zero filling	1.25×10^{-3} cm^{-1}
SNR in the involved spectral domain	≈ 1000
Collimator focal length	1040 mm
Nominal iris radius	2.00 mm
Free spectral range	5266-7899 cm^{-1}
Involved spectral domain	7000-7500 cm^{-1}

Spectrum number	Effective iris radius (mm) [a]	Total pressure ±0.5% [b] (hPa)	Absorbing path ±1 cm [b]	Temperature ±0.5 K [b]
1	1.89(4)	79.98	3216.6	295.15
2	1.89(4)	39.95	3216.6	295.15
3	1.84(6)	13.59	3216.6	296.65
4	1.90(4)	6.414	3216.6	296.45
5	1.94(5)	1.949	3216.6	295.85
6	1.82(6)	13.55	2416.6	295.35
7	1.87(5)	5.350	2416.6	295.55
8	1.89(4)	3.336	2416.6	295.35
9	1.89(4)	1.998	2416.6	295.25
10	1.93(6)	1.333	2416.6	295.35
11	1.65(4)	13.38	421.6	294.45
12	1.83(3)	5.332	421.6	293.75
13	1.85(3)	2.655	421.6	293.85
14	1.86(6)	1.336	421.6	293.85
15	1.83(3)	0.661	421.6	293.75

[a] 1 SD between parentheses in unit of the last digit.
[b] Absolute uncertainty (excess digits are given as a guide).

Table 3
Experimental conditions and characteristics of the spectra recorded in the 1.4-μm region using the rapid-scan interferometer in Paris (LADIR)

Commercial sample (Air Liquide Alphagaz)	
Natural C_2H_2	97.760% of $^{12}C_2H_2$
Stated purity	99.55%
Maximum path difference	90 cm
Unapodized FWHM resolution	$\approx 5.6 \times 10^{-3}$ cm^{-1}
Spectral step after post-zero filling	3.77×10^{-3} cm^{-1}
SNR in the involved spectral domain	≈ 1000
Collimator focal length	418 mm
Nominal iris radius	0.40 mm
Free spectral range	5500-11000 cm^{-1}
Involved spectral domain	7000-7500 cm^{-1}

Spectrum number	Effective iris radius (mm) [a]	Total pressure ±0.5% [b] (hPa)	Absorbing path ±1 cm [b]	Temperature ±0.5 K [b]
16	0.45(1)	3.224	2015	296.95
17	0.45(1)	8.316	2015	296.95
18	0.45(1)	9.361	2015	296.00
19	0.45(1)	16.56	2015	296.95
20	0.45(1)	20.72	2015	296.00
21	0.45(1)	26.43	2015	296.95
22	0.45(1)	46.03	2015	298.15
23	0.45(1)	53.20	2015	296.00
24	0.45(1)	92.20	2015	296.00

[a] 1 SD between parentheses in unit of the last digit.
[b] Absolute uncertainty (excess digits are given as a guide).

Table 4
Line positions and intensities for bands of the $^{12}C_2H_2$ molecule in the 1.4 μm region [a]

Line	Position	S_{obs}	S_{calc}	%	$\|R\|^2_{obs}$
$2\nu_1 + \nu_5{}^1$					
Pee31	7330.87670	9.524E-25	1.001E-24	-5.10	8.292E-07
Pee30	7334.03491	4.608E-25	4.567E-25	0.89	8.738E-07
Pee27	7343.35162	3.257E-24	3.256E-24	0.03	8.499E-07
Pee25	7349.43101	5.480E-24	5.437E-24	0.78	8.451E-07
Pee24	7352.43112	2.317E-24	2.297E-24	0.86	8.404E-07
Pee23	7355.40497	8.681E-24	8.613E-24	0.78	8.339E-07
Pee21	7361.27303	1.302E-23	1.292E-23	0.77	8.221E-07
Pee20	7364.16711	5.215E-24	5.168E-24	0.90	8.178E-07
Pee19	7367.03482	1.837E-23	1.834E-23	0.16	8.061E-07
Pee18	7369.87576	7.138E-24	7.123E-24	0.21	8.006E-07
Pee17	7372.68992	2.466E-23	2.454E-23	0.49	7.971E-07
Pee16	7375.47711	9.286E-24	9.250E-24	0.39	7.905E-07
Pee15	7378.23795	3.106E-23	3.087E-23	0.61	7.863E-07
Pee14	7380.97159	1.126E-23	1.126E-23	0.00	7.756E-07
Pee12	7386.35844	1.282E-23	1.279E-23	0.23	7.659E-07
Pee11	7389.01185	4.008E-23	3.972E-23	0.90	7.649E-07
Pee10	7391.63728	1.376E-23	1.342E-23	2.47	7.715E-07
Pee 9	7394.23575	4.087E-23	3.979E-23	2.64	7.664E-07
Pee 8	7396.80772	1.285E-23	1.276E-23	0.70	7.453E-07
Pee 7	7399.35237	3.643E-23	3.570E-23	2.00	7.493E-07
Pee 6	7401.86953	1.076E-23	1.065E-23	1.02	7.356E-07
Pee 5	7404.35972	2.762E-23	2.718E-23	1.59	7.339E-07
Pee 4	7406.82248	7.143E-24	7.136E-24	0.10	7.169E-07
Pee 3	7409.25802	1.491E-23	1.482E-23	0.60	7.147E-07
Qfe29	7408.65966	3.194E-24	3.167E-24	0.85	6.977E-07
Qfe27	7409.67704	5.727E-24	5.660E-24	1.17	7.001E-07
Qfe25	7410.62233	9.655E-24	9.613E-24	0.44	6.949E-07
Qfe24	7411.06801	4.100E-24	4.096E-24	0.10	6.925E-07
Qfe23	7411.49566	1.550E-23	1.550E-23	0.00	6.918E-07
Qfe22	7411.90532	6.431E-24	6.436E-24	-0.08	6.914E-07
Qfe21	7412.29666	2.445E-23	2.372E-23	2.99	7.131E-07
Qfe20	7412.67101	9.332E-24	9.584E-24	-2.70	6.737E-07
Qfe19	7413.02657	3.415E-23	3.437E-23	-0.64	6.874E-07
Qfe18	7413.36447	1.318E-23	1.350E-23	-2.43	6.754E-07
Qfe17	7413.68437	4.638E-23	4.708E-23	-1.51	6.816E-07
Qfe16	7413.98679	1.756E-23	1.797E-23	-2.33	6.762E-07
Qfe15	7414.27100	6.038E-23	6.081E-23	-0.71	6.870E-07
Qfe14	7414.53759	2.187E-23	2.251E-23	-2.93	6.722E-07
Qfe12	7415.01675	2.524E-23	2.642E-23	-4.68	6.609E-07
Qfe11	7415.22977	8.304E-23	8.367E-23	-0.76	6.867E-07
Qfe10	7415.42492	2.849E-23	2.887E-23	-1.33	6.827E-07
Qfe 9	7415.60234	8.756E-23	8.789E-23	-0.38	6.893E-07
Qfe 8	7415.76194	2.857E-23	2.906E-23	-1.72	6.803E-07
Qfe 7	7415.90378	8.352E-23	8.428E-23	-0.91	6.857E-07
Qfe 6	7416.02800	2.599E-23	2.638E-23	-1.50	6.818E-07
Qfe 5	7416.13427	7.048E-23	7.171E-23	-1.75	6.800E-07
Qfe 2	7416.34715	1.176E-23	1.246E-23	-5.95	6.529E-07
Qfe 1	7416.38254	2.223E-23	2.295E-23	-3.24	6.701E-07

Table 4 (continued)

Line	Position	S_{obs}	S_{calc}	%	$\|R\|^2_{obs}$
Ree 0	7418.72597	5.115E-24	5.116E-24	-0.02	6.857E-07
Ree 1	7421.02418	2.248E-23	2.256E-23	-0.36	6.772E-07
Ree 2	7423.29496	9.878E-24	9.715E-24	1.65	6.848E-07
Ree 3	7425.53816	3.500E-23	3.488E-23	0.34	6.695E-07
Ree 4	7427.75353	1.360E-23	1.321E-23	2.87	6.806E-07
Ree 5	7429.94145	4.355E-23	4.328E-23	0.62	6.590E-07
Ree 6	7432.10146	1.549E-23	1.525E-23	1.55	6.588E-07
Ree 7	7434.23385	4.803E-23	4.707E-23	2.00	6.556E-07
Ree 8	7436.33841	1.596E-23	1.576E-23	1.25	6.443E-07
Ree 9	7438.41519	4.672E-23	4.648E-23	0.51	6.334E-07
Ree10	7440.46409	1.511E-23	1.493E-23	1.19	6.314E-07
Ree11	7442.48515	4.244E-23	4.236E-23	0.19	6.187E-07
Ree12	7444.47828	1.361E-23	1.313E-23	3.53	6.335E-07
Ree13	7446.44338	3.602E-23	3.601E-23	0.03	6.052E-07
Ree14	7448.38060	1.083E-23	1.080E-23	0.28	6.006E-07
Ree15	7450.28973	2.866E-23	2.870E-23	-0.14	5.916E-07
Ree16	7452.17083	8.328E-24	8.346E-24	-0.22	5.848E-07
Ree17	7454.02386	2.139E-23	2.154E-23	-0.70	5.758E-07
Ree18	7455.84874	6.084E-24	6.087E-24	-0.05	5.732E-07
Ree19	7457.64557	1.516E-23	1.527E-23	-0.73	5.631E-07
Ree20	7459.41424	4.211E-24	4.195E-24	0.38	5.630E-07
Ree21	7461.15455	1.026E-23	1.024E-23	0.19	5.558E-07
Ree22	7462.86674	2.706E-24	2.738E-24	-1.18	5.418E-07
Ree23	7464.55070	6.506E-24	6.507E-24	-0.02	5.419E-07
Ree25	7467.83375	3.908E-24	3.924E-24	-0.41	5.272E-07
Ree27	7471.00323	2.282E-24	2.247E-24	1.53	5.247E-07
$\nu_1 + \nu_2 + (2\nu_4 + \nu_5)^1$					
Pee19	7180.97929	2.939E-24	2.713E-24	7.69	1.323E-07
Pee18	7183.60242	1.207E-24	1.199E-24	0.66	1.389E-07
Pee17	7186.20934	4.320E-24	4.633E-24	-7.25	1.432E-07
Pee15	7191.37289	6.005E-24	7.071E-24	-17.75	1.560E-07
Pee11	7201.52499	1.232E-23	1.201E-23	2.52	2.413E-07
Pee10	7204.02649	4.435E-24	4.266E-24	3.81	2.552E-07
Pee 9	7206.51635	1.338E-23	1.323E-23	1.12	2.575E-07
Pee 7	7211.45733	1.328E-23	1.274E-23	4.07	2.803E-07
Pee 6	7213.90651	4.080E-24	3.905E-24	4.29	2.861E-07
Pee 3	7221.16706	5.687E-24	5.696E-24	-0.16	2.796E-07
Qfe22	7225.63343	2.432E-24	2.213E-24	9.00	2.682E-07
Qfe21	7225.87729	7.538E-24	8.241E-24	-9.33	2.255E-07
Qfe19	7226.33139	1.156E-23	1.216E-23	-5.19	2.387E-07
Qfe17	7226.73996	1.829E-23	1.695E-23	7.33	2.757E-07
Qfe16	7226.92944	7.032E-24	6.517E-24	7.32	2.777E-07
Qfe15	7227.09990	2.120E-23	2.221E-23	-4.76	2.474E-07
Qfe14	7227.25949	7.267E-24	8.277E-24	-13.90	2.291E-07
Qfe12	7227.54104	9.661E-24	9.831E-24	-1.76	2.595E-07
Qfe11	7227.66230	3.048E-23	3.129E-23	-2.66	2.586E-07
Qfe10	7227.77065	1.090E-23	1.085E-23	0.46	2.680E-07
Qfe 9	7227.86729	3.378E-23	3.317E-23	1.81	2.728E-07

Table 4 (continued)

Line	Position	S_{obs}	S_{calc}	%	$\|R\|^2_{obs}$
Qfe 7	7228.02661	3.238E-23	3.204E-23	1.05	2.727E-07
Qfe 6	7228.08941	1.033E-23	1.006E-23	2.61	2.780E-07
Qfe 4	7228.18517	8.060E-24	7.929E-24	1.63	2.763E-07
Qfe 1	7228.26543	8.754E-24	8.820E-24	-0.75	2.707E-07
Ree 1	7232.93319	8.292E-24	8.434E-24	-1.71	2.563E-07
Ree 2	7235.23656	3.534E-24	3.551E-24	-0.48	2.514E-07
Ree 3	7237.51964	1.248E-23	1.239E-23	0.72	2.450E-07
Ree 4	7239.79045	4.507E-24	4.531E-24	-0.53	2.314E-07
Ree 5	7242.04601	1.396E-23	1.423E-23	-1.93	2.167E-07
Ree 6	7244.28693	4.937E-24	4.773E-24	3.32	2.154E-07
Ree 7	7246.51420	1.337E-23	1.389E-23	-3.89	1.873E-07
Ree 8	7248.72747	4.128E-24	4.353E-24	-5.45	1.710E-07
Ree10	7253.11325	3.587E-24	3.500E-24	2.43	1.537E-07
Ree11	7255.28345	8.212E-24	8.980E-24	-9.35	1.228E-07
Ree12	7257.43908	2.257E-24	2.480E-24	-9.88	1.078E-07
Ree13	7259.57867	5.529E-24	5.959E-24	-7.78	9.531E-08
Ree14	7261.70192	1.516E-24	1.534E-24	-1.19	8.625E-08
Ree15	7263.80860	3.510E-24	3.414E-24	2.74	7.433E-08
Ree16	7265.89777	9.141E-25	8.061E-25	11.81	6.583E-08
Ree17	7267.96851	2.036E-24	1.621E-24	20.38	5.623E-08
$2\nu_3 + \nu_5{}^1$					
Pee33	7129.17268	9.646E-25	9.779E-25	-1.38	1.699E-06
Pee31	7135.29242	1.837E-24	1.839E-24	-0.11	1.643E-06
Pee28	7144.28476	1.447E-24	1.440E-24	0.48	1.543E-06
Pee27	7147.23268	5.660E-24	5.599E-24	1.08	1.517E-06
Pee26	7150.15665	2.422E-24	2.389E-24	1.36	1.487E-06
Pee25	7153.05506	9.241E-24	9.051E-24	2.06	1.464E-06
Pee24	7155.92958	3.788E-24	3.761E-24	0.71	1.412E-06
Pee23	7158.78055	1.401E-23	1.388E-23	0.93	1.383E-06
Pee21	7164.40985	2.018E-23	2.020E-23	-0.10	1.309E-06
Pee20	7167.18970	7.904E-24	7.949E-24	-0.57	1.274E-06
Pee19	7169.94607	2.770E-23	2.779E-23	-0.32	1.249E-06
Pee18	7172.67862	1.052E-23	1.064E-23	-1.14	1.212E-06
Pee16	7178.07980	1.339E-23	1.341E-23	-0.15	1.171E-06
Pee14	7183.38988	1.573E-23	1.587E-23	-0.89	1.113E-06
Pee12	7188.61308	1.745E-23	1.752E-23	-0.40	1.071E-06
Pee10	7193.75079	1.738E-23	1.788E-23	-2.88	1.002E-06
Pee 8	7198.80488	1.561E-23	1.659E-23	-6.28	9.300E-07
Pee 6	7203.77576	1.302E-23	1.351E-23	-3.76	9.144E-07
Pee 5	7206.23073	3.424E-23	3.404E-23	0.58	9.350E-07
Pee 3	7211.07902	1.789E-23	1.814E-23	-1.40	8.809E-07
Pee 2	7213.47248	3.047E-24	3.069E-24	-0.72	8.695E-07
Qfe27	7212.09316	6.249E-24	6.218E-24	0.50	7.848E-07
Qfe26	7212.53479	2.726E-24	2.734E-24	-0.29	7.829E-07
Qfe25	7212.99142	1.024E-23	1.068E-23	-4.30	7.570E-07
Qfe23	7213.78672	1.739E-23	1.740E-23	-0.06	7.971E-07
Qfe22	7214.16248	7.321E-24	7.255E-24	0.90	8.086E-07
Qfe21	7214.52080	2.686E-23	2.685E-23	0.04	8.051E-07
Qfe19	7215.18535	3.909E-23	3.925E-23	-0.41	8.084E-07

Table 4 (continued)

Line	Position	S_{obs}	S_{calc}	%	$\|R\|^2_{obs}$
Qfe18	7215.49104	1.591E-23	1.548E-23	2.70	8.372E-07
Qfe16	7216.05420	2.112E-23	2.074E-23	1.80	8.355E-07
Qfe14	7216.54844	2.647E-23	2.615E-23	1.21	8.358E-07
Qfe13	7216.77098	8.553E-23	8.595E-23	-0.49	8.239E-07
Qfe12	7216.97696	3.069E-23	3.086E-23	-0.55	8.255E-07
Qfe11	7217.16639	9.851E-23	9.794E-23	0.58	8.369E-07
Qfe10	7217.33971	3.442E-23	3.387E-23	1.60	8.474E-07
Qfe 8	7217.63808	3.427E-23	3.421E-23	0.18	8.385E-07
Qfe 7	7217.76353	1.014E-22	9.931E-23	2.06	8.558E-07
Qfe 4	7218.04434	2.445E-23	2.450E-23	-0.20	8.392E-07
Qfe 3	7218.10659	5.920E-23	5.988E-23	-1.15	8.320E-07
Qfe 2	7218.15376	1.557E-23	1.477E-23	5.14	8.879E-07
Qfe 1	7218.18499	2.573E-23	2.720E-23	-5.71	7.969E-07
Ree 0	7220.53252	6.089E-24	6.001E-24	1.45	8.386E-07
Ree 4	7229.65982	1.507E-23	1.494E-23	0.86	7.746E-07
Ree 5	7231.88941	4.914E-23	4.854E-23	1.22	7.639E-07
Ree 6	7234.09831	1.731E-23	1.697E-23	1.96	7.566E-07
Ree 9	7240.59664	5.088E-23	5.062E-23	0.51	7.087E-07
Ree10	7242.71886	1.610E-23	1.616E-23	-0.37	6.911E-07
Ree11	7244.81919	4.632E-23	4.562E-23	1.51	6.935E-07
Ree12	7246.89659	1.416E-23	1.406E-23	0.71	6.774E-07
Ree13	7248.95156	3.844E-23	3.837E-23	0.18	6.636E-07
Ree14	7250.98317	1.162E-23	1.146E-23	1.38	6.617E-07
Ree15	7252.99252	3.028E-23	3.035E-23	-0.23	6.420E-07
Ree16	7254.97392	8.984E-24	8.798E-24	2.07	6.479E-07
Ree17	7256.93533	2.291E-23	2.264E-23	1.18	6.334E-07
Ree18	7258.87133	6.315E-24	6.382E-24	-1.06	6.112E-07
Ree19	7260.78280	1.625E-23	1.598E-23	1.66	6.201E-07
Ree20	7262.66901	4.433E-24	4.387E-24	1.04	6.087E-07
Ree21	7264.52997	1.084E-23	1.069E-23	1.38	6.034E-07
Ree22	7266.36535	2.916E-24	2.862E-24	1.85	5.995E-07
Ree23	7268.17459	6.862E-24	6.802E-24	0.87	5.870E-07
Ree25	7271.71496	4.114E-24	4.113E-24	0.02	5.700E-07
Ree27	7275.14875	2.332E-24	2.368E-24	-1.54	5.506E-07
Ree28	7276.82479	5.645E-25	5.881E-25	-4.18	5.320E-07
Ree31	7281.68987	6.438E-25	6.795E-25	-5.55	5.130E-07
$\nu_1 + \nu_3 + \nu_4{}^1$					
Pee35	7042.78226	4.219E-25	4.249E-25	-0.71	1.555E-06
Pee34	7046.06223	2.060E-25	2.019E-25	1.99	1.574E-06
Pee33	7049.31838	8.508E-25	8.523E-25	-0.18	1.516E-06
Pee32	7052.54448	3.993E-25	3.951E-25	1.05	1.511E-06
Pee31	7055.74213	1.586E-24	1.627E-24	-2.59	1.435E-06
Pee30	7058.91218	7.247E-25	7.352E-25	-1.45	1.428E-06
Pee25	7074.38177	8.692E-24	8.336E-24	4.10	1.393E-06
Pee23	7080.38039	1.298E-23	1.295E-23	0.23	1.295E-06
Pee22	7083.33786	5.298E-24	5.271E-24	0.51	1.277E-06
Pee21	7086.26775	1.880E-23	1.904E-23	-1.28	1.233E-06
Pee20	7089.18320	7.365E-24	7.535E-24	-2.31	1.200E-06
Pee19	7092.05439	2.635E-23	2.647E-23	-0.46	1.201E-06

Table 4 (continued)

Line	Position	S_{obs}	S_{calc}	%	$\|R\|^2_{obs}$
Pee18	7094.90370	1.031E-23	1.018E-23	1.26	1.201E-06
Pee16	7100.52112	1.304E-23	1.294E-23	0.77	1.153E-06
Pee14	7106.02959	1.492E-23	1.544E-23	-3.49	1.067E-06
Pee12	7111.42846	1.712E-23	1.715E-23	-0.18	1.062E-06
Pee 8	7121.89629	1.625E-23	1.638E-23	-0.80	9.787E-07
Pee 6	7126.96452	1.338E-23	1.337E-23	0.07	9.498E-07
Pee 5	7129.45704	3.352E-23	3.371E-23	-0.57	9.252E-07
Pee 4	7131.92196	8.896E-24	8.751E-24	1.63	9.272E-07
Qfe27	7135.02819	6.562E-24	6.622E-24	-0.91	8.329E-07
Qfe26	7135.49176	2.848E-24	2.895E-24	-1.65	8.268E-07
Qfe25	7135.93864	1.116E-23	1.124E-23	-0.72	8.342E-07
Qfe22	7137.17919	7.431E-24	7.528E-24	-1.31	8.297E-07
Qfe21	7137.55382	2.733E-23	2.775E-23	-1.54	8.277E-07
Qfe20	7137.91305	1.116E-23	1.121E-23	-0.45	8.367E-07
Qfe18	7138.58042	1.536E-23	1.580E-23	-2.86	8.170E-07
Qfe15	7139.45333	7.121E-23	7.114E-23	0.10	8.413E-07
Qfe14	7139.70959	2.746E-23	2.634E-23	4.08	8.764E-07
Qfe13	7139.94904	8.647E-23	8.633E-23	0.16	8.419E-07
Qfe12	7140.17121	3.074E-23	3.092E-23	-0.59	8.357E-07
Qfe11	7140.37614	9.777E-23	9.787E-23	-0.10	8.396E-07
Qfe10	7140.56402	3.388E-23	3.378E-23	0.30	8.430E-07
Qfe 8	7140.88832	3.424E-23	3.399E-23	0.73	8.467E-07
Qfe 7	7141.02498	9.924E-23	9.858E-23	0.67	8.461E-07
Qfe 4	7141.33157	2.391E-23	2.422E-23	-1.30	8.297E-07
Qfe 3	7141.40038	5.910E-23	5.917E-23	-0.12	8.395E-07
Qfe 2	7141.45127	1.471E-23	1.458E-23	0.88	8.478E-07
Qfe 1	7141.48562	2.637E-23	2.685E-23	-1.82	8.255E-07
Ree 0	7143.82887	6.226E-24	5.912E-24	5.04	8.667E-07
Ree 1	7146.12523	2.562E-23	2.576E-23	-0.55	8.015E-07
Ree 3	7150.63567	3.849E-23	3.886E-23	-0.96	7.644E-07
Ree 4	7152.84878	1.481E-23	1.454E-23	1.82	7.694E-07
Ree 6	7157.19029	1.616E-23	1.635E-23	-1.18	7.139E-07
Ree 9	7163.49114	4.811E-23	4.791E-23	0.42	6.772E-07
Ree10	7165.53457	1.511E-23	1.518E-23	-0.46	6.556E-07
Ree12	7169.53641	1.281E-23	1.299E-23	-1.41	6.195E-07
Ree13	7171.49479	3.463E-23	3.513E-23	-1.44	6.043E-07
Ree14	7173.42494	1.058E-23	1.039E-23	1.80	6.091E-07
Ree16	7177.19888	7.645E-24	7.804E-24	-2.08	5.573E-07
Ree17	7179.04412	1.988E-23	1.984E-23	0.20	5.556E-07
Ree19	7182.64154	1.425E-23	1.364E-23	4.28	5.499E-07
Ree20	7184.40027	3.707E-24	3.693E-24	0.38	5.146E-07
Ree21	7186.13020	9.113E-24	8.872E-24	2.64	5.126E-07

[a] Bands are listed in the same order as in Table 1. The quoted line position is the measured one in cm^{-1}. S_{obs} and S_{calc} are measured and calculated intensities, respectively, for pure $^{12}C_2H_2$ (i.e., for a sample containing 100% of $^{12}C_2H_2$), in cm·molecule^{-1} at 296 K. % is the ratio $100 \times (S_{obs} - S_{calc}) / S_{obs}$. $|R|^2_{obs}$ is the experimental transition dipole moment squared value, in D^2 (1 D = 3.33546×10^{-30} C·m), deduced from S_{obs}.

Table 5
Summary of $^{12}C_2H_2$ experimental vibrational transition dipole moments squared $|R_0|^2$ in D^2 (1 D = 3.33546×10^{-30} C·m), and Herman-Wallis coefficients, see Eqs. (5,6), for 4 bands in the 1.4 μm spectral region [a]

Band	$\|R_0\|^2$ in D^2	A_1^{RP}	A_2^{RP}	A_2^{Q}
$2\nu_1 + \nu_5^1$	$6.919(36) \times 10^{-7}$	$-4.42(16) \times 10^{-3}$	$-1.54(85) \times 10^{-5}$	
$\nu_1 + \nu_2 + (2\nu_4 + \nu_5)^1$	$2.728(65) \times 10^{-7}$	$-8.5(10) \times 10^{-3}$	$-1.364(84) \times 10^{-3}$	$-1.12(61) \times 10^{-4}$
$2\nu_3 + \nu_5^1$	$8.424(67) \times 10^{-7}$	$-9.56(17) \times 10^{-3}$	$+1.051(94) \times 10^{-4}$	$-5.1(15) \times 10^{-5}$
$\nu_1 + \nu_3 + \nu_4^1$	$8.405(52) \times 10^{-7}$	$-1.043(19) \times 10^{-2}$		

[a] 95% confidence intervals (2 SD, in unit of the last quoted digit) are given between parenthesis. For $|R_0|^2$ values, the overall accuracy is ±5%. Non given Herman-Wallis coefficients have been fixed at zero.

Table 6
Summary of bands and transitions now available for the $^{12}C_2H_2$ molecule

Spectral region (μm)	Number of bands [a] cold / hot	Number of transitions [a] cold / hot	Spectral domain (cm^{-1})	Intensity range ($cm \cdot molecule^{-1}$ at 296 K)
13.6 [b,c]	1 / 5	150 / 1038	604- 870	10^{-18} - 10^{-26}
7.7 [b,c]	1 / 0	71 / 0	1248-1415	10^{-19} - 10^{-22}
5 [b,c]	3 / 15	283 / 1212	1810-2255	10^{-22} - 10^{-25}
3.8 [d]	2 / 3	90 / 331	2499-2769	10^{-21} - 10^{-25}
3 [b,c]	2 / 0	125 / 0	3204-3359	10^{-19} - 10^{-21}
3 [e]	0 / 18	77[f] / 1971	3139-3398	10^{-20} - 10^{-26}
2.5 [d]	4 / 5	450 / 720	3762-4226	10^{-21} - 10^{-27}
2.2 [e]	4 / 4	254 / 392	4421-4798	10^{-22} - 10^{-25}
1.9 [e]	7 / 0	539 / 0	5032-5567	10^{-24} - 10^{-26}
1.7 [e]	2 / 4	175 / 350	5692-6032	10^{-23} - 10^{-26}
1.5 [b]	2 / 2	129 / 224	6448-6685	10^{-20} - 10^{-24}
1.5 [e]	4 / 16	200 / 1443	6277-6865	10^{-23} - 10^{-28}
1.4 [e]	4 / 0	347 / 0	7042-7476	10^{-22} - 10^{-25}

Band [g]	Origin [g]	ν_{min} - ν_{max} [g]	ΣS [g]	S_{min} - S_{max} [g]	$J_{max}\nu/J_{max}S/J_{max}$ [g]			Cdν [g] CdS [g]
3 μm spectral region								
100101__–000011	3239.73	3139-3308	2.1E-20	2.5E-25-5.6E-22	38-31	23-21	38-31	3/- 5/4
010312_2–000202	3257.31	3164-3335	1.6E-20	4.4E-25-4.6E-22	37-34	18-14	37-34	3/- 5/4
010310+2–000200+	3258.46	3160-3335	1.1E-20	2.3E-25-5.6E-22	39-33	21-21	39-33	3/- 5/4
010220–_–000110–	3259.23	3176-3326	5.7E-21	1.3E-24-2.9E-22	33-29	17-12	33-29	3/- 5/4
010222_2–000112	3260.47	3167-3326	7.7E-21	2.1E-25-2.1E-22	37-28	16-10	37-28	3/- 5/4
010130+2–000020+	3261.63	3207-3309	1.9E-21	5.9E-24-1.1E-22	22-20	11- 7	22-20	3/- 5/4
010132_2–000022	3262.83	3191-3332	4.4E-21	1.4E-24-1.2E-22	29-30	17-11	29-30	3/- 5/4
010211_2–000101	3269.54	3146-3367	4.1E-19	8.8E-26-1.0E-20	47-43	34-31	48-44	3/- 6/5
010121_2–000011	3272.10	3155-3368	1.9E-19	8.0E-26-4.9E-21	46-42	28-24	46-43	3/- 6/5
001202__–000202	3275.72	3182-3352	2.1E-20	5.8E-25-5.8E-22	37-34	21-14	37-34	3/- 5/4
001112__–000112	3277.25	3202-3347	1.3E-20	3.9E-24-3.4E-22	30-30	22-21	30-30	3/- 5/4
001110–_–000110–	3277.37	3202-3342	7.2E-21	2.9E-24-3.7E-22	30-28	21-15	30-28	3/- 5/4
001200+_–000200+	3277.64	3188-3348	1.0E-20	1.1E-24-5.0E-22	35-31	21-21	35-31	3/- 5/4
001020+_–000020+	3277.95	3210-3336	5.0E-21	6.6E-24-2.6E-22	27-25	13-17	27-25	3/- 5/4
001022__–000022	3278.02	3201-3347	7.2E-21	1.3E-24-1.9E-22	31-30	22-17	31-30	3/- 5/4
001110+_–000110+	3281.26	3211-3341	8.0E-21	8.5E-24-4.1E-22	28-26	20-16	28-26	3/- 5/4
010110+_–000000+	3281.90	3151-3387	5.0E-18	3.8E-25-2.5E-19	52-51	39-39	50-50	4/- 6/5
001101__–000101	3285.47	3162-3383	4.4E-19	1.2E-25-1.2E-20	47-46	31-31	47-46	3/- 6/5
001011__–000011	3286.38	3165-3386	2.8E-19	5.0E-26-7.2E-21	46-48	32-30	46-48	3/- 6/5
001000+_–000000+	3294.84	3162-3398	4.4E-18	2.2E-25-2.2E-19	53-51	41-37	50-50	4/- 6/5

Table 6 (continued)

Band [g]	Origin [g]	ν_{min} - ν_{max} [g]	ΣS [g]	S_{min} - S_{max} [g]	$J_{max}\nu/J_{max}S/J_{max}$ [g]			Cdν [g]	CdS [g]
2.2 μm spectral region									
010310+_–000000+	4488.81	4421-4565	1.4E-21	3.8E-25-7.0E-23	29-30	29-30	30-30	4/4	5/5
010411__–000101	4489.92	4443-4554	2.7E-22	2.5E-25-7.2E-24	20-18	18-18	25-25	4/3	6/5
001200+_–000000+	4508.01	4438-4583	8.2E-22	1.7E-25-4.3E-23	29-29	29-29	30-30	4/3	6/5
001301__–000101	4511.71	4451-4579	1.6E-22	1.2E-25-4.3E-24	25-22	21-18	25-25	4/3	6/5
100121__–000011	4652.40	4590-4714	1.9E-22	1.3E-25-5.8E-24	20-23	20-22	25-25	4/3	6/5
100211__–000101	4656.86	4595-4729	3.3E-22	9.2E-26-9.4E-24	22-22	22-22	25-30	4/3	5/4
100110+_–000000+	4673.65	4585-4552	2.3E-21	1.5E-25-1.3E-22	29-29	29-29	35-35	4/3	6/5
001020+_–000000+	4727.07	4654-4798	6.4E-22	1.5E-25-3.7E-23	26-27	26-25	30-30	4/3	6/5
1.9 μm spectral region									
001301__–000000+	5102.80	5032-5167	8.5E-23	1.2E-25-4.4E-24	25-19	25-19	30-25	3/3	6/5
					21	21	25	4/3	6/5
010411_2–000000+	5124.57	5050-5183	6.1E-23	1.3E-26-3.1E-24	25-19	25-19	30-25	4/3	6/5
					25	25	30	4/3	6/5
020110+_–000000+	5230.23	5135-5293	1.5E-22	1.9E-26-7.3E-24	29-24	29-24	35-30	4/3	6/5
011000+_–000000+	5260.02	5164-5322	1.9E-22	2.7E-26-9.5E-24	29-24	29-24	35-30	4/3	6/5
100211_1–000000+	5290.28	5230-5350	1.4E-22	6.8E-26-7.7E-24	19-21	19-21	25-25	4/3	6/5
					27	27	30	4/3	6/5
010231_3–000000+	5302.30	5239-5370	6.0E-23	1.5E-26-2.8E-24	21-25	21-25	25-30	4/3	6/5
					23	23	27	4/3	6/5
100031__–000000+	5510.40	5447-5567	4.2E-23	1.8E-26-2.1E-24	19-23	19-23	25-25	4/3	6/5
					25	25	30	4/3	6/5
1.7 μm spectral region									
002000+_–000011	5774.24	5692-5835	6.8E-23	1.7E-26-3.4E-24	26-28	20-14	30-30	4/3	6/5
					25	23	25	4/4	6/6
110200+_–000011	5786.00	5721-5841	6.0E-23	4.0E-26-3.1E-24	20-16	20-16	25-25	4/3	6/5
					21	21	25	4/3	6/5
020211_2–000000+	5815.69	5735-5878	5.5E-23	1.2E-26-2.7E-24	30-27	17-19	30-30	4/4	6/5
					23	23	25	4/3	6/5
011101__–000000+	5849.47	5769-5911	2.2E-22	4.4E-26-1.1E-23	29-27	23-23	30-30	4/3	6/5
					29	25	30	4/3	6/5
101000+_–000101	5945.93	5849-6014	9.6E-23	3.8E-27-4.6E-24	31-32	23-21	35-35	4/3	6/5
					33	24	35	4/3	6/5
200000+_–000011	5981.03	5897-6032	4.6E-23	1.7E-26-2.3E-24	26-24	14-14	30-25	4/4	6/5
					29	21	30	4/4	6/5
1.5 μm spectral region									
002202__–000112	6342.62	6277-6396	4.7E-24	6.0E-27-1.4E-25	25-19	17-13	25-25	4/3	5/5
002110+_–000020+	6355.89	6318-6391	9.7E-25	3.5E-27-6.6E-26	15-13	15- 9	15-15	4/3	4/4
002101__–000011	6362.12	6279-6425	5.4E-23	1.2E-26-1.4E-24	31-28	24-21	31-30	4/3	6/5
020310+_–000000+	6413.90	6360-6462	4.5E-23	1.4E-25-2.5E-24	22-20	21-17	22-20	4/3	6/5
011200+_–000000+	6449.10	6388-6509	3.1E-22	3.3E-25-1.7E-23	24-22	24-22	25-25	4/3	6/5

Table 6 (continued)

Band [g]	Origin [g]	ν_{min} - ν_{max} [g]	ΣS [g]	S_{min} - S_{max} [g]	$J_{max}\nu/J_{max}S/J_{max}$ [g]			Cdν [g]	CdS [g]
101200+_–000200+	6502.38	6421-6538	4.3E-22	2.1E-25-2.4E-23	27-15	26-10	30-15	4/3	6/5
101202__–000202	6503.52	6422-6565	9.3E-22	2.9E-25-2.6E-23	28-27	28-26	30-30	4/3	6/5
101112__–000112	6504.90	6453-6549	5.9E-22	1.6E-24-1.8E-23	20-18	15-17	20-20	4/3	4/4
101110+_–000110+	6506.91	6425-6567	3.1E-22	1.8E-25-1.6E-23	28-27	26-21	30-30	4/3	6/5
101020+_–000020+	6512.71	6431-6573	1.8E-22	7.8E-26-9.4E-24	28-25	27-23	30-30	4/3	5/5
101110–_–000110–	6512.73	6415-6581	3.4E-22	3.6E-26-1.8E-23	35-33	33-23	35-35	4/3	6/5
101022__–000022	6513.22	6431-6574	3.1E-22	7.0E-26-8.5E-24	27-25	25-18	30-30	4/3	5/5
101101__–000101	6529.80	6448-6587	2.3E-20	5.2E-24-6.1E-22	30-28	30-28	30-28	4/-	7/-
101011__–000011	6534.74	6459-6593	1.3E-20	4.9E-24-3.3E-22	28-28	28-28	28-28	4/-	7/-
101000+_–000000+	6556.47	6542-6627	2.6E-19	1.3E-23-1.3E-20	37-37	37-37	37-37	4/3	6/5
200101__–000011	6567.21	6468-6634	1.2E-21	5.2E-26-3.2E-23	34-32	31-32	35-35	4/3	6/5
110211_2–000101	6594.25	6514-6661	8.6E-22	1.8E-25-2.2E-23	32-30	27-26	30-30	4/3	6/5
110121_2–000011	6600.18	6519-6667	2.5E-22	4.9E-26-6.6E-24	26-27	21-27	30-30	4/3	6/5
002011__–000101	6606.50	6527-6670	4.2E-22	1.1E-25-1.2E-23	29-30	25-29	30-30	4/3	6/5
110211_1–000101	6616.57	6552-6673	2.5E-22	4.4E-28-8.4E-24	25-23	22-22	25-25	4/3	5/5
110110+_–000000+	6623.14	6564-6686	3.2E-21	1.2E-24-1.7E-22	23-30	23-30	23-30	4/-	7/-
020130+_–000000+	6654.25	6604-6703	4.5E-23	1.5E-25-2.5E-24	20-21	17-21	20-21	4/3	6/5
011020+_–000000+	6690.57	6614-6763	1.2E-22	1.6E-26-6.1E-24	30-33	25-25	30-33	4/3	6/5
200011__–000101	6804.69	6722-6865	3.7E-23	8.2E-27-9.6E-25	28-28	23-23	30-30	4/3	6/5
1.4 μm spectral region									
101101__–000000+	7142.67	7042-7193	2.0E-21	1.9E-25-1.0E-22	35-22	35-21	35-25	4/3	6/5
					29	27	30	4/3	6/5
002011__–000000+	7219.37	7122-7282	2.1E-21	2.2E-25-1.0E-22	33-31	33-31	35-31	4/3	6/5
					27	27	27	4/-	6/-
110211__–000000+	7229.45	7178-7274	5.3E-22	9.4E-26-3.2E-23	19-17	19-17	20-20	4/3	6/6
					22	22	25	4/3	6/6
200011__–000000+	7417.57	7317-7476	1.7E-21	1.2E-25-8.6E-23	31-27	31-27	35-30	4/3	6/5
					29	29	35	4/3	6/5

[a] $^{12}C^{13}CH_2$ data are not mentioned ; [b] HITRAN 2004 ; [c] GEISA 2003 ; [d] HITRAN updates of 2007.

[e] New data from the present work.

[f] New high J lines added to the 2 cold bands already presented in HITRAN 2004 and GEISA 2003 (see Section 3.2).

[g] Explanation of the column headings:

Band: vibrational assignment used in the line lists, according to Section 2.1: v_1 v_2 v_3 v_4 v_5 $\ell \pm r$ for the upper and lower states (when $\pm$ or r does not occur for the upper state, it is replaced by an underlined space).

Origin: approximate value of the band center, in cm^{-1}.

ν_{min} - ν_{max} : limiting values of line positions, in cm^{-1}.

ΣS : sum of line intensities, in cm·molecule^{-1} at 296 K.

S_{min} - S_{max} : limiting values of line intensities, in cm·molecule^{-1} at 296 K.

$J_{max}\nu$: maximum value of J for which a line position has been measured.

$J_{max}S$: maximum value of J for which a line intensity has been measured.

J_{max} : maximum value of J present in the line list.

(The first value is for the P-branch and the second for the R-branch. When a value is on a separate line, it concerns the Q-branch of the above band.)

Cdν: uncertainty code for line positions [2]. Code 3: 10^{-3}-10^{-2} cm^{-1}. Code 4: 10^{-4}-10^{-3} cm^{-1}.

CdS: uncertainty code for line intensities [2]. Code 4: 10-20%. Code 5: 5-10%. Code 6: 2-5%. Code 7 : 1-2%.

(The second value is for interpolated or extrapolated lines if any. These uncertainty codes are typical values, more severe codes can exceptionally occur for some lines.)
Other spectroscopic data are the same as those already put in the last updates of the databases: air- and self-broadening coefficients, default value for the temperature exponent of air-broadening coefficients, constant value for the air-pressure shifting coefficient, and their accuracies [2,6,22].

Table 7
Corrected line intensities and $|R|^2$ values for some Q lines of the $\nu_3+\nu_4{}^1$ band of $^{12}C_2H_2$ in the 2.5-μm region [a]

Line	Position	S_{obs}	S_{calc}	%	$\|R\|^2_{obs}$
Qfe27	3896.45930	1.46E-22	1.48E-22	-1.37	3.40E-5
Qfe26	3896.54321	6.49E-23	6.53E-23	-0.62	3.45E-5
Qfe25	3896.61922	2.49E-22	2.55E-22	-2.41	3.41E-5
Qfe24	3896.68752	1.09E-22	1.09E-22	0.00	3.52E-5
Qfe23	3896.74893	4.14E-22	4.16E-22	-0.48	3.51E-5
Qfe22	3896.80383	1.80E-22	1.74E-22	3.33	3.67E-5
Qfe21	3896.85270	6.55E-22	6.41E-22	2.14	3.64E-5
Qfe20	3896.89589				
Qfe19	3896.93436				

[a] The quoted line position is the measured one in cm^{-1}. S_{obs} and S_{calc} are measured and calculated intensities, respectively, for pure $^{12}C_2H_2$ (i.e., for a sample containing 100% of $^{12}C_2H_2$), in cm·molecule^{-1} at 296 K. % is the ratio $100 \times (S_{obs} - S_{calc}) / S_{obs}$. $|R|^2_{obs}$ is the experimental transition dipole moment squared value, in D^2 (1 D = 3.33546×10^{-30} C·m), deduced from S_{obs}. The listed results should replace those given for the corresponding lines in Table 4 of [7].

Table 8
Additional $^{12}C_2H_2$ experimental vibrational transition dipole moments squared $|R_0|^2$ in D^2 (1 D = 3.33546×10^{-30} C·m), and Herman-Wallis coefficients, see Eq. (4) of [10], for 6 bands in the 2.2 μm spectral region [a]

Band	Center [b]	$\|R_0\|^2$	A_1^{RP}	A_2^{RP}
$\nu_2+(3\nu_4+\nu_5)^0{}_+$	4488.810	$9.292(80) \times 10^{-7}$	$-3.00(30) \times 10^{-3}$	$-3.28(20) \times 10^{-4}$
$\nu_3+2\nu_5{}^0$	4727.067	$4.135(20) \times 10^{-7}$	$+9.09(20) \times 10^{-3}$	$-3.24(15) \times 10^{-4}$
$\nu_3+2\nu_4{}^0$	4508.010	$5.908(30) \times 10^{-7}$	$-2.65(20) \times 10^{-3}$	$-5.7\ (15) \times 10^{-4}$
$\nu_1+(2\nu_4+\nu_5)^1 - \nu_4{}^1$	4656.858	$4.113(20) \times 10^{-6}$	$+8.62(35) \times 10^{-3}$	
$\nu_2+(4\nu_4+\nu_5)^1 - \nu_4{}^1$	4489.920	$3.732(20) \times 10^{-6}$	$-3.90(50) \times 10^{-3}$	
$\nu_3+3\nu_4{}^1 - \nu_4{}^1$	4511.708	$2.283(30) \times 10^{-6}$	$-4.04(70) \times 10^{-3}$	$-3.37(70) \times 10^{-4}$

[a] 95% confidence intervals (2 SD, in unit of the last quoted digit) are given between parenthesis. For $|R_0|^2$ values, the overall accuracy is around ±7%. Non given Herman-Wallis coefficients have been fixed at zero.
[b] Rough values of band centers, in cm^{-1}, are given as a guide.

Fig. 1. Variation of the transition dipole moment squared $|R|^2$, in D^2 ($1\ D = 3.33546 \times 10^{-30}$ C·m), vs. *m*, for the $2\nu_1 + \nu_5{}^1$ band (solid triangles are for *P*- and *R*-branches, and open triangles for the *Q*-branch). The solid lines have been calculated using the constants found in this work (see Table 5).

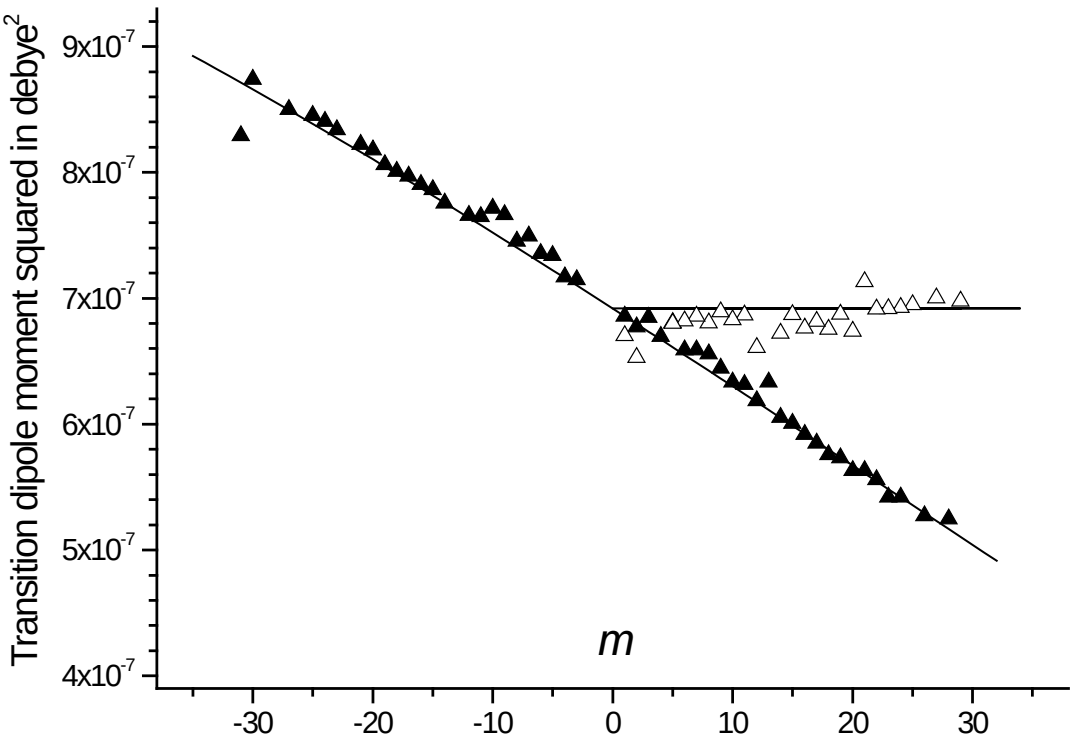

Fig. 2. Line intensity ranges in each spectral domain of $^{12}C_2H_2$ (marked by their ΔP value). Upper plot: data present in the HITRAN 2004 issue, with the updates of 2007. Lower plot: data now available for databases after the present work.